J Infrared Milli Terahz Waves (2012) 33:97–126
DOI 10.1007/s10762-011-9865-7

Review of Moisture and Liquid Detection and Mapping using Terahertz Imaging

John F. Federici

Received: 23 August 2011 / Accepted: 9 December 2011 /
Published online: 28 January 2012

Abstract The relatively high permittivity of liquid water compared to other materials in the Terahertz (THz) range enables a contrast mechanism for the detection and imaging of moisture. In this paper, spatial mapping of moisture and liquid detection by THz imaging is reviewed. Analysis of the moisture content is discussed in terms of a double Debye model for liquid water and effective medium models for the permittivity of the dry and 'wet' materials of interest. Examples from medical applications, forestry products, agriculture/ food products, and polymers are reviewed. Extraction of diffusion rates and diffusion maps from THz images are discussed.

Keywords Terahertz · Non-destructive evaluation · Water · Diffusion · Moisture · Humidity

1 Introduction

Researchers who are unfamiliar with Terahertz (THz) technology typically first learn two basic facts concerning the propagation of THz: THz radiation does not readily penetrate through metals nor polar liquids such as water. While these facts do pose some limitations for THz technology when it is applied the detection of concealed weapons/explosives [1, 2] as well as wireless communications, [3, 4] the limitations of THz propagation through water does enable one of the most useful applications of THz imaging: the detection of moisture or humidity in materials. What makes this application such a natural fit for THz imaging is that water is highly absorptive in the THz range, while most materials which absorb moisture are either very transparent (eg. paper, plastics) or reasonably transparent to THz. Consequently, there is a high contrast in the image between 'moist' and 'dry' regions. While this review focuses mostly on the detection and diffusion mapping of water, clearly the same principles can be applied to the detection and diffusion of other liquids. As long as the permittivity of the liquid is much higher than that of the surrounding materials, the high contrast between the 'wet' and 'dry' material enables detection and diffusion mapping of the liquid.

Typical time-scales for water diffusion in materials are on the order of hours or days. Since state-of-the-art THz imaging systems can scan objects in much shorter time periods

J. F. Federici (✉)
Department of Physics, New Jersey Institute of Technology, Newark, NJ 07102, USA
e-mail: federici@adm.njit.edu

(typically a few to tens of seconds), the speed of THz imaging hardware is not a critical issue for diffusion mapping. Another property of THz imaging which fosters its use for the mapping of diffusion is its ability to resolve structures comparable in size to the electromagnetic wavelength of the THz radiation. Typical spatial resolutions for ~1THZ radiation are limited by diffraction effects to ~300 μm which enables one to image water diffusion into comparably-sized cracks and voids in concrete, natural cork, composite plastics, and other materials. While the presence of small cracks in materials may not create a large contrast in 'dry' THz absorbance images, the penetration of a liquid with high permittivity into those cracks will produce an enhanced contrast in 'wet' THz absorbance images.

A moisture map of a drying leaf [5, 6] is widely accepted to be the first demonstration of THz imaging. From these first measurements, other examples of moisture or liquid detection using THz techniques have emerged. For example, advances in the analysis of THz transmission through leaves has enabled the non-invasive, in-situ measurement of hydration levels in plant leaves which may enable effective monitoring and allocation of water resources for agriculture. The large THz reflectivity due to high water content in fruit such as grapes has lead to the development of THz imaging as a non-invasive methodology to predict crop yields. The central role of water to biological function makes the detection of water via THz imaging an effective technique in medical applications as well as non-destructive evaluation of agricultural products such as grain and pecans. For example, imaging of skin cancer and thermal damage to skin (burns) have been extensively studied with THz. The contrast mechanism results from different hydration levels in normal versus cancerous tissue and healthy versus thermally damaged skin.

The potential of THz technology for 2-D moisture detection is extensive. Using 2-D THz technology, one can create images of liquid diffusion fronts in a host material, extract average diffusion coefficients, observe local and anisotropic variations in the diffusion coefficient, and non-destructively assess hydration levels in materials. While examples of water diffusion measurements in 2-D are abundant, the water's absorbance is too large to permit 3-D THz imaging of thick samples to be feasible. However, if the THz absorbance of a 'dry' image is dominated by the internal structures of the material, one can use a THz image of the internal structures as a 3-D map of preferred diffusion pathways. For example, the cracks, voids, fissures, and scratches in materials may represent routes of rapid water diffusion. Based on the presence and organization of these defects, the diffusion of water through the structure can be numerically predicted as if the sample were exposed to water.

The paper is organized as follows: Section 2 describes the modeling of THz propagation through hydrated material. The modeling analysis includes discussion of relevant optical parameters and contrast mechanisms, the Double Debye model for the permittivity of water, effective medium models which describe the effective permittivity for a 'host' material which has absorbed water, as well as the effects of scattering. The extraction of diffusion coefficients using THz imaging is detailed in Section 3. The remaining sections summarize various applications of THz moisture detection to medicine (Section 4), forestry products (paper, wood, and natural cork Section 5), plastics and composites (Section 6), agriculture and food (Section 7), and other materials. The important advancements and near-term expectations for the field are summarized in Section 9.

2 Modeling of the effective permittivity of water in a host material

Terahertz techniques typically take advantage of the fact that most common THz systems [7–9] enable one to measure both the phase and amplitude of the THz radiation. The phase and

amplitude of a THz electric field propagating as a plane wave in the+z direction as a function of time t can be expressed as

$$E = E_0 \exp(ik\tilde{n}z - i2\pi\nu t) \tag{1}$$

where the initial amplitude of the wave is E_0, the vacuum wavenumber is $k=2\pi/\lambda$, $\tilde{n}$ is the complex index of refraction, λ is the electromagnetic wavelength, and ν is the frequency of the THz wave in a vacuum, respectively. The complex index of refraction can alternatively be expressed in terms of the complex dielectric ε such that $\tilde{n} = \sqrt{\varepsilon}$. Expanding Eq. (1) in terms of the real and imaginary part of the complex refractive index $\tilde{n}=n_r+in_i$ gives $E=E_0 \exp(-kn_iz)\exp(ikn_rz - i\omega t)$. The first exponential corresponds to damping of the wave's magnitude through the imaginary index of refraction while the second exponential describes the changing phase of the wave through the real index of refraction. Alternatively, one can define the attenuation coefficient (in electric field) as $\alpha=kn_i$ so that

$$E = E_0 \exp(-kn_iz) \exp(ikn_rz - i\omega t) = E_0 \exp(-\alpha z) \exp(ikn_rz - i\omega t) \tag{2}$$

The complex dielectric permittivity is related to the real refractive index and absorption coefficient α through $\varepsilon=\tilde{n}^2=(n_r+in_i)^2$ and $n_i=\alpha\lambda/2\pi$ such that

$$\varepsilon = \varepsilon_r \pm i\varepsilon_i = \left[{n_r}^2 - \left(\frac{\alpha\lambda}{2\pi}\right)^2\right] + i\left[n_r \frac{\alpha\lambda}{\pi}\right]. \tag{3}$$

(The absorption coefficient of power is 2α.) The introduction of the $\pm$ sign in Eq. (3) will be discussed below.

2.1 Contrast mechanism

The high permittivity of liquid water is typically the dominate contrast mechanism for moisture detecting by THz imaging. For example, typical real indices of refraction and absorption coefficients at 1 THz for wood [10] (n~1.3, α~15 cm^{-1}), leaves (solid material) [11] (n~1.7, α~40 cm^{-1}), polyamide plastic [12] (n~1.75, α~10 cm^{-1}), and cork cell walls [13] (n~1.2, α~10 cm^{-1}), are smaller than that of water (n~2, α~230 cm^{-1}). Note that the absorption coefficients for liquid water are typically an order of magnitude or more larger than most other materials. The permittivity of liquid water in the THz range exhibits only very broad spectral features. Consequently, the addition of water to a host material typically increases the overall absorbance at all THz frequencies without introducing any strong/ narrow spectral features. As is noted in Section 2.3, there is a slight difference in the permittivities of free liquid water and water molecules which are weakly bound to another material.

2.2 THz response of water – Debye model

There have been numerous papers and review articles concerning the frequency dependent THz permittivity of liquid water. A good overview of the topic including the Debye model is given in [14, 15]. In the THz range, the complex permittivity of liquid water is typically described as a sum of low pass filters which represent a sum of relaxation times. For the THz range, the sum is limited typically to two terms and called a double Debye model. In this model, the complex frequency dependant permittivity is modeled as

$$\varepsilon_w(\nu) = \varepsilon_\infty + \frac{\varepsilon_o - \varepsilon_1}{1 \pm i2\pi\nu\tau_1} + \frac{\varepsilon_1 - \varepsilon_\infty}{1 \pm i2\pi\nu\tau_2} \tag{4}$$

where ε_∞ is the high frequency limit of the permittivity, ε_o and ε_1 are constants, while the time constants refer to temperature-dependant slow (τ_1), and fast (τ_2) relaxation processes. Below 100 GHz, a single Debye term is sufficient to describe water. [16] The ± signs in Eq. (4) and Eq. (3) are included to highlight the fact that definitions of the equations for the complex dielectric coefficient and complex refractive index will vary in the scientific literature. As a result of the different definitions, the resulting imaginary contribution to the permittivity can either be positive or negative depending upon the definitions of Eqs. (3) and (4).

The permittivity of water is modeled using Eq. (4) assuming Debye parameters for 'free' liquid water. However, it has been recognized that polar water molecules may interact and weakly bond to polar functional groups on the surface of the host material. The weak bonding of 'bound' water to the host's surface modifies the vibrations of the water molecules leading to a lower refractive index and absorption coefficient. There are challenges to including both the bound and free water contributions into an effective medium model: It is difficult to experimentally separate the contributions of bound and free water to the permittivity. In certain cases, such as water absorption by polyamide and wood-plastic composite, the measurement is simplified by the fact that only bound water exists in these materials assuming that one is well below the fiber saturation point. [12]

2.3 Effective medium models

In calculating the THz absorption by a hydrated host material, one is naturally led to consider the measured effective permittivity of the water/ host combination. If the permittivity of 'pure' water ε_w and host material ε_h (ie. dry material) are individually known, an effective medium model can be used, in conjunction with their respective volume fractions, to combine the permittivities of the water and 'host' material into an effective permittivity which represents the response of the 'wet' material (Fig. 1). Regardless of the particular effective medium model which is used to describe a material, the goal of the analysis is to use the measured THz optical constants from the effective medium model to determine the volume fraction of water.

In order to describe the effective dielectric properties of mixtures in the Terahertz range, several methods have been proposed. [11–13, 16] As an example, [17] used a simple mixing model which incorporates the presence of water via a linear model for the effective absorption coefficient and the volume fraction of water :

$$\alpha_{eff}(\nu) = X_h\alpha_h(\nu) + X_w\alpha_w(\nu) \tag{5}$$

where *eff* stands for the effective medium, *h* stands for the host medium and *w* stands for the water. For a two component system, $X_h+X_w=1$.

The physical origin of the mixing model Eq. (5) can be explained using Fig. 1. In this illustration, the 'host' material is embedded with small particles. Conceptually, the 'particle' material is agglomerated into a uniform layer for which the equivalent structure is as shown in Fig. 1b with a host and particle layer thickness denoted by L_h and L_p . The total thickness is L. The thickness of the layers are chosen such that the volume factions of the 'host' and 'particle' materials in Fig. 1a and b are the same. If one were to neglect reflective losses compared to attenuation losses, then the effective absorbance of Fig. 1b should be $\alpha_{eff}(\nu)L = L_h\alpha_h(\nu)+L_p\alpha_p(\nu)$. Dividing both sides of the equation by the total length of the sample L yields

$$\alpha_{eff}(\nu) = \frac{L_h}{L}\alpha_h(\nu) + \frac{L_p}{L}\alpha_p(\nu) = X_h\alpha_h(\nu) + X_p\alpha_p(\nu) \tag{6}$$

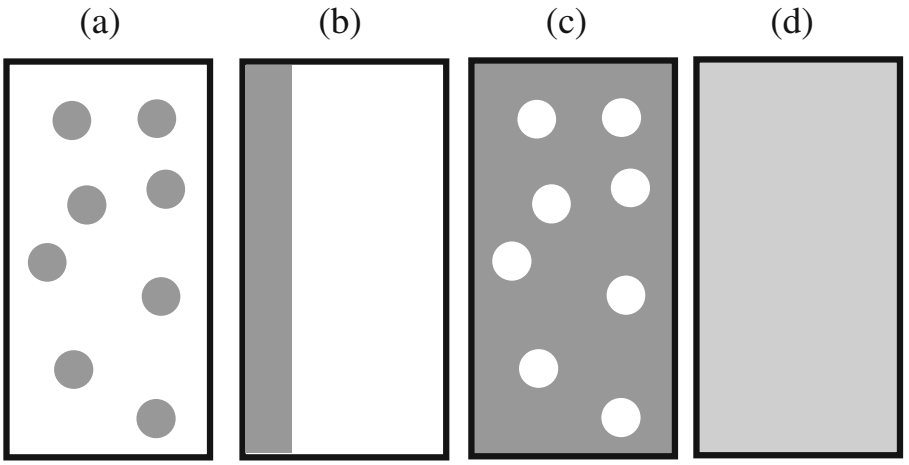

Fig. 1 Schematic representation of (**a**) a host material embedded with particles of water. (**b**) Equivalent effective material in the mixing model in which all of the particles are agglomerated to a single layer of thickness L_p. (**c**) An 'inverse' material consisting of a water host embedded with particles of another dielectric (**d**) The effective medium comprised of a uniform material with effective dielectric ε_{eff}.

which is just Eq. (5) in which 'particles' of water are embedded in a host medium. If one were to switch the labels of 'host' and 'water' such that $h \rightarrow w$ and $w \rightarrow h$, this would correspond to a water 'host' embedded with particles of another dielectric material (Fig. 1c). It should be noted that the simple mixing model Eq. (5) is symmetric, meaning that the effective absorption coefficient is unchanged when the roles of 'host' and 'particle' are exchanged. The goal of the various effective medium models is to treat the embedded particles in the host material as exhibiting a uniform effective dielectric as illustrated in Fig. 1d.

Some of the more widely used effective medium models include the Maxwell-Garnet (MG), Bruggeman (BG), and Landau-Lifshitz-Looyenga (LLL) models. All of these models attempt to account for local electric field effects which occur when the presence of the particles perturb the electric field from an electromagnetic wave as it interacts with an individual, isolated particle. Higher order interactions among the particles are neglected. It is assumed that the electromagnetic field averages over spatial scales which are large compared to the particle size.

Maxwell-Garnett theory [18] calculates the effective dielectric properties of a material formed by the presence of small (spherical) particles embedded in a host material:

$$\frac{\varepsilon_{eff} - \varepsilon_h}{\varepsilon_{eff} + 2\varepsilon_h} = X_p \frac{\varepsilon_p - \varepsilon_h}{\varepsilon_p + 2\varepsilon_h} \tag{7}$$

where the subscripts h and p represent the 'host' and 'particle', and X_p is the volume fraction of the 'particles'. It is further assumed in the MG model that the volume faction of the 'particles' is small so that size of the particles is much smaller than the spacing between the particles. The MG model is asymmetric with respect to exchanging the roles of 'host' and 'particle'.

The BG model [19] is an extension of the MG model which enables one to calculate the effective permittivity of N components in a mixture. In terms of the volume fraction and

permittivity of N individual components, the effective permittivity in this model for spherical particles may be written as

$$\sum_{j=1}^{N} X_j \left(\frac{\varepsilon_{eff} - \varepsilon_j}{\varepsilon_j + 2\varepsilon_{eff}} \right) = 0 \tag{8}$$

where the volume fractions are constrained by $\sum_{j=1}^{N} X_j = 1$. For a two component medium in which $X_h + X_p = 1$, Eq. (8) can be rewritten as

$$\varepsilon_{eff} = \frac{1}{4} \left(\beta + \sqrt{\beta^2 + 8\varepsilon_h \varepsilon_p} \right) \tag{9}$$

where

$$\beta = (3X_h - 1)\varepsilon_h + (3X_p - 1)\varepsilon_p. \tag{10}$$

Note that the BG model is symmetric with respect to exchanging the roles of the 'host' and 'particle' components. In comparing the BG versus MG model, it is expected that the BG model would be more accurate as the volume fraction of the particles increases since it treats both the host and particles symmetrically. It should be noted that [16] uses an asymmetric version of the BG model which was misprinted. The correct formula should be

$$X_p = 1 - \frac{\varepsilon_p - \varepsilon_{eff}}{\varepsilon_p - \varepsilon_h} \left(\frac{\varepsilon_h}{\varepsilon_{eff}} \right)^{1/3}. \tag{11}$$

The symmetric BG model assumes a mixture of two types of spherical particles while the asymmetric BG model, as well as the MG model, assumes that the particles are embedded in an otherwise uniform host material as illustrated in Fig. 1a.

For the LLL model the effective dielectric permittivity is modeled as

$$\sqrt[3]{\varepsilon_{eff}} = X_h \sqrt[3]{\varepsilon_h} + X_p \sqrt[3]{\varepsilon_p}. \tag{12}$$

One disadvantage of the LLL model is that it is derived in the limit of low dielectric contrast mixtures and technically can only be applied in this limit. However, the advantage of the LLL model compared to MG and BG models is that the embedded particles are not assumed to have any particular shape. As with the symmetric BG and mixing model (Eq. (5)), the LLL model is symmetric with respect is exchanging the role of the 'host' and water materials.

As pointed out by Kaatze and Hubner [16], there are a plethora of effective medium models which extend the MG or BG models given above from spherical particles to ellipsoidal, needle-like, or disk-like, particles. Depending on the model chosen, the predicted effective permittivity for the same volume fractions and permittivity of the 'host' and 'particle' materials may differ significantly from model to model. Following the review of Kaatze and Hubner [16], Figure 2 compares the effective medium models of MG, BG (both symmetric and asymmetric), and LLL for mixtures of spherically shaped particles with dielectric constant ε_p in a 'host' of water with dielectric constant ε_w. As seen in Fig. 2, the various models give different predictions of the effective permittivity. The BG relation assumes that the material close to a particle is characterized by the mixture permittivity ε_{eff} so that the Bruggeman relation should apply for large values of X_p corresponding to a small

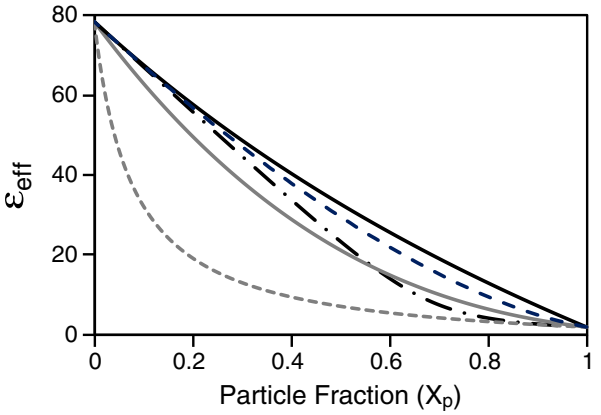

Fig. 2 Based on [16], a graphical representation of effective medium models for two component mixtures of dielectric particles dispersed in liquid water host. The particles are assumed to be spherical in shape with ε_p=2 and volume fraction X_p. The permittivity of water is 78.35. The solid black line is the MG formula (Eq. (7)), the dashed black line is the asymmetric BG relation (Eq. (11)) while the dash-dot line is the symmetric BG relation (Eq. (8)). The solid gray line is the LLL relation (Eq. (12)). While the inverse MG relation – which represents spherical particles of water in a dielectric host material – is represented by the gray dashed line.

volume fraction of water. Kaatze and Hubner [16] note that experimental data for mixtures of water and non-polar constituents normally follows the MG and asymmetric BG formula over a wide range of volume fractions of the host material. This is surprising since Eqs. (7) and (11) are asymmetric with respect to the exchange of 'host' and 'particle' for a two component system.

The MG effective medium model is asymmetric with regards to switching the roles of 'host' and 'particles'. The 'inverse' MG model of Fig. 2 is a plot of Eq. (7) in which the role of the 'host' and 'particles' are reversed such that $h \rightarrow p$, $p \rightarrow h$, and $X_p \rightarrow 1 - X_p$. This would represent a mixture of spherical water particles in a dielectric host material. The mixture of water particles in a dielectric host experiences stronger effects of depolarizing electric fields [16] compared to dielectric particles in water. Consequently, the effective permittivity of the water particle/ host mixture is significantly smaller than dielectric particles embedded in water as a host. Therefore, Kaatze and Hubner [16] argue that the mixture of a small amount of water in a host material should follow the prediction of an inverse effective permittivity model, such as the 'inverse' MG model. Figure 2 shows that the symmetric BG model closely follows the MG model at low particle fractions, while the symmetric BG model closely follows the inverse MG model at high particle fractions. Kaatze and Hubner note that depending on the system of interest, different effect models provide best fits to experimental data. For example, the LLL model, which is also symmetric, does not agree with experimental findings for mixtures of nonpolar materials with water, but works well with compressed samples made from pulverized powders. In the THz literature on moisture sensing, it is common to try several different effective medium models and then choose the model which best fits the experimental data.

2.4 Scattering

It is well know that scattering of electromagnetic radiation in the THz range can be considerable since the spatial scale of refractive index fluctuations - due to variations in either the surface roughness or internal structure of a material - can become comparable to the THz wavelength.[20] In this section, two aspects of scattering are discussed: (a) the

effect of surface roughness and scattering on the effective medium models and (b) the effect of scattering on THz imaging as it relates to water detection.

Since all of the effective medium models discussed in Section 2.3 are solutions to Maxwell's electromagnetic equations in the static limit for which the electromagnetic wavelength is larger than the typical spatial scale of the medium, the effect of scattering is not included in the effective medium models. Scattering by the roughness of layers in a host material and its effect on the measured THz attenuation must be explicitly added to the analysis. Jordens *et. al* [11] included the effect of interface roughness of a leaf into their analysis by defining an effective attenuation coefficient of the leaf as a sum of absorptive and scattering losses:

$$\alpha_{total} = \alpha_{abs} + \alpha_{scat} \tag{13}$$

where the THz wavelength dependant scattering coefficient as evaluated from a Rayleigh roughness factor [21] is

$$\alpha_{scat}(\lambda) = \frac{1}{D}\left[\left(\sqrt{\varepsilon_L(\lambda)} - 1\right)\left(\frac{4\pi\,\Gamma\cos\theta}{\lambda}\right)\right]^2 \tag{14}$$

where D is the thickness of the leaf, Γ is the standard deviation of the height profile (measure of surface roughness), θ is the angle of incidence, λ is the THz free space wavelength, and ε_L is the wavelength dependant permittivity of the leaf.

The relatively strong contribution of scattering to the total measured absorbance can be either an asset or a liability for moisture detection by THz imaging. Typically, one thinks of scattering as a limitation for THz imaging: the edges of structures are not well defined. Variations in the refractive index can steer the THz beam resulting in distorted or blurred images. While this certainly is of concern for moisture sensing, water detection has the advantage that the dielectric constant of water is large compared to that of most materials of interest. Therefore, while THz images through a material might be blurred due to scattering by local variations in the refractive index, the presence of moisture can still be detected due to the high dielectric contrast between water and the host material.

There are many applications of THz imaging for non-destructive evaluation [13, 22–25] for which the contrast mechanism results from enhanced scattering by cracks, voids, and defects in an otherwise isotropic material. The diffusion of water in these materials, such as natural cork (Section 5.3) and concrete (Section 8.2) preferentially tend to follow the channels formed by the cracks, voids, and defects. In this case, an image of the enhanced absorbance due to scattering in the *dry* material can indicate locations of high water diffusion in the wet material. In Section 5.3, it is shown that a dry THz absorbance image can be used to predict the diffusion of water through the material.

2.5 Extraction of moisture level from transmission or reflection data

The extraction of a moisture level from the experimental data is typically done assuming a particular transmission or reflection model. A common model is to assume that the transmission is measured through a slab of effective medium material of thickness L which is surrounded by air with an assumed permittivity of unity. In terms of the effective complex refractive index, the THz transmission at normal incidence can be written as

$$T(\nu) \equiv \frac{E_t(\nu)}{E_o(\nu)} = \frac{\left(4\widetilde{n}/(\widetilde{n}+1)^2\right)e^{i\widetilde{n}2\pi\nu L/c}}{1-((\widetilde{n}-1)/(\widetilde{n}+1))^2 e^{i4\widetilde{n}\pi\nu L/c}} \tag{15}$$

where c is the speed of light, ν is the THz frequency, and $\tilde{n} = \sqrt{\varepsilon_{eff}}$ is the complex effective refractive index derived from the effective medium models in Section 2.3. In applications for which the sample is optically thick - such as hydration studies of biological tissues - rendering transmission measurements impractical, alternatively one can utilize a reflective approach. The THz reflectivity at normal incidence from an optically thick material of refractive index $\tilde{n}$ can be expressed from a simple Fresnel reflection equation [14]

$$r(\nu) \equiv \frac{E_r(\nu)}{E_o(\nu)} = \frac{1-\tilde{n}}{1+\tilde{n}}. \tag{16}$$

The moisture level enters the THz transmission and reflection equations through the contribution of water to the effective permittivity. From the known permittivity of water and dry host material, Equations (4)-(16) are used to fit the experimentally measured transmission or reflection to one of the effective medium models in which the volume water content is one of the fitting parameters.

3 Extraction of diffusion coefficients using THz imaging

As will be discussed in Sections 4–8, there have been many papers and examples concerning the detection of moisture in materials, as well as THz absorbance images which can interpreted as spatial maps of the local water content. However, relatively few papers analyze the time evolution of these spatial maps to extract either an average or local diffusion coefficient. In this section, calculations of diffusion coefficients using THz imaging are reviewed.

While the well-known diffusion equation

$$\frac{\partial C}{\partial t} = \vec{\nabla}\left(D\vec{\nabla}C\right) \tag{17}$$

can be easily written, this formulation – in which C is the concentration of the diffusing material (eg. liquid water) and D is the diffusion coefficient – shelters a variety of subtleties in the diffusion process. For example, the diffusion coefficient D can depend on the concentration of water. Measurements of water diffusion in cellulose, [26] which is the main component of paper, suggests that there is 'immobile' water which is bound to the cellulose fibers. Free water which is not weakly bound to the fibers is more mobile. Consequently, the diffusion rate of water is cellulose should increase with concentration as one approaches the fiber saturation point since the volume fraction of 'mobile' water molecules increases. The diffusion coefficient D can also be anisotropic (ie. a tensor) as well as spatially dependant. A perfect example of an anisotropic and inhomogeneous diffusion coefficient is natural cork (Section 5.3).

To date, the only experimental THz method which has been used to extract diffusion coefficients from absorbance data is THz time-domain systems. Both reflective and transmission geometries have been employed. An example of a reflective geometry for the extraction of diffusion coefficients is the measurement of acetone diffusion in polycarbonate and polyvinylchloride polymers [27]. In these measurements, a THz reflection geometry is used to track the progression of the dry polymer/liquid interface over time. Pulses of THz radiation reflect from dry polymer/liquid interface. As the boundary of the diffusing liquid moves through the material, the reflecting pulses are detected earlier in time indicating

motion of the liquid. In analyzing the kinetics of the wavefront, the diffusion is modeled by the time-dependant position $d(t)$ of the penetrating liquid/dry polymer interface

$$d(t) = K' \, t^{m} \tag{18}$$

where K' and m are constants and t is time.

THz time-domain systems in the transmission mode have been used to measure the diffusion of solvents in polymeric materials [12] such as polyamide and wood plastic composite. Figure 3 below shows the measured water absorption (in weight %) as a function of time for polyamide and wood-plastic composite. As described in [12], the diffusion is modeled using the weight percent increase in the sample

$$Wt\%(t) = K \, t^{m} \tag{19}$$

where K and m are constants and t is time. When $m=1/2$, the diffusion follows Fick diffusion. THz absorbance values are converted to equivalent water concentrations based on an effective medium model for the 'wet' sample. Equations (18) and (19) are essentially the same within multiplicative scaling factors K and K': Since the location of the liquid/dry polymer interface should be correlated with a threshold value of the liquid's local concentration, both the reflective and transmission geometry can be used in conjunction with Eqs. (18) or (19) to extract a diffusion coefficient. A fit of the measured total water absorption versus time in polyamide follows the Fick diffusion model with a diffusion coefficient of 3.4×10^{-13} m^2/s. The fit of wood-plastic composite data yields an exponent of $m> 1/2$ which is attributed to the compound mixture of plastic with wood.

As another example of liquid diffusion measurements in a THz transmission geometry, [13] measured the time dependant diffusion through a thin disk of natural cork. The diffusion process can be modeled using the solution to the diffusion equation Eq. (17) for a radial geometry corresponding to diffusion of water through an isotropic disk with a constant fluid concentration along its radius a: [28]

$$\frac{M_t}{M_\infty} = 1 - \sum_{n=1}^{\infty} \frac{4}{a^2\sigma_n^2} \cdot e^{-D\sigma_n^2(t-t_0)} \tag{20}$$

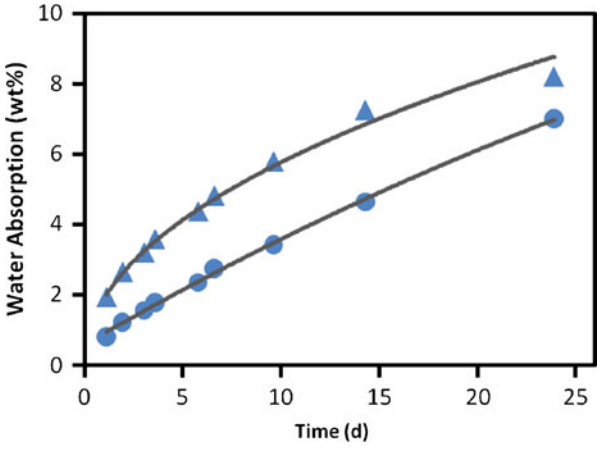

Fig. 3 Water absorption of polyamide (triangle) and wood-plastic composite (circle) as a function of time. Solid lines are fits to the experimental data. Adapted from [12].

where M_t and M_∞ are the amount of diffusing water at time t and $t=\infty$, respectively. The disk has a radius a and an effective diffusion coefficient D. The coefficients σ_n are chosen such that $a\sigma_n$ is the n-th root of the zeroth order Bessel function J_o of the first kind, such that $J_o(a\sigma_n)=0$.

While the above examples show that the average diffusion coefficient in a sample can be extracted from THz absorbance, the measurements can not be used directly to extract a local diffusion coefficient, for example, using Eq. (20): the 'boundary' of a localized area is not well defined and the water concentration at the boundary is dynamic and not controlled during the experiment. Due to dynamic conditions around any single location in the sample, one needs to use modeling and simulation to assess the localized diffusion coefficient. To date, there have been no detailed comparisons of the experimentally measured time-progression of liquid diffusion by THz imaging with modeling or simulations of the diffusion process.

Conceptually, one method for determining the local diffusion coefficient is to invert Eq. (17) and use the measured concentration of water as a function of time and position to extract the locally varying diffusion coefficient. The mathematical complexity of this approach is multiplied by the realistic expectation that the local diffusion constant is anisotropic and in the case of cellulose [26], can also depend on water concentration. An alternative approach is to utilize the THz dry image as a basis for creating a diffusion coefficient map of the material. Depending on the contrast mechanism in the dry THz image, this approach may be viable. For example it is well-know that the presence of voids, cracks, scratches, and other defects in an otherwise homogenous sample can lead to contrast in a THz absorbance image due to enhanced THz scattering by these defects. In that case, regions of preferential diffusion should also correspond to regions of high THz absorbance due to enhanced scattering in the dry THz images. In essence a dry THz image can be converted into a map of the local diffusion coefficient. If such a map were realistic, then one use this diffusion coefficient map to numerically integrate Eq. (17) and compare the resulting time-dependant maps of water concentration to the absorbance maps as measured by THz imaging.

As a simple implementation, a two-value diffusion coefficient could be used. For THz absorbance above a fixed threshold, the diffusion coefficient is assumed to be high corresponding to the presence of cracks or voids in the sample structure. For THz absorbance of the dry image below the threshold, the diffusion coefficient could be assumed to be an order of magnitude smaller. One would expect that this two value model would be appropriate, for example, for a homogeneous sample in which THz imaging detects the presence of cracks or voids. Water would diffuse rapidly through the cracks and voids, but progresses much more slowly in homogeneous regions of the sample. The relative magnitude of the two values of the local diffusion coefficient can be constrained so that the average diffusion coefficient for the entire sample is consistent with the value extracted from Fick diffusion equation solutions such as Eqs. (18)–(20).

Using the two value diffusion map, the diffusion Eq. (17) could be numerically integrated in time at each pixel position to calculate the updated water concentration value as a function of position and time. For comparison of the diffusion equation's numerical solution to the experimentally measured THz absorbance, one can extract the location of the water diffusion wavefront by processing the THz absorbance images to monitor which pixels exhibit an absorbance value above a fixed threshold. The concentration images generated from numerical solutions of the diffusion equation can be converted to absorbance images by either knowing the calibration between water concentration and THz absorbance from experimental measurements or by application of effective medium models as described in Section 2. Applying the same threshold absorbance to the simulated diffusion images allows the direct

comparison of the experimental and simulated water diffusion wavefronts. The application of a two-value diffusion map to water diffusion in cork will be discussed in Section 5.3.

4 Medical applications

A recent review article [14] presented a comprehensive summary of hydration sensing in medicine. In the present review only the most salient points are addressed for completeness. As pointed out in [14] and cited references in that review paper, there are two reasons for the prevalence of water as the contrasting mechanism in THz medical imaging: (a) the prevalence of water in physiological tissues and (b) the large permittivity of water relative to the other constituents in biological systems. Due to the limited propagation of THz through liquid water, reflective THz imaging is preferable to transmission imaging. Luckily, THz reflectivity is very sensitive to small changes in hydration levels. THz studies of different types of healthy and cancerous tissues show that the variations in the dielectric or permittivity properties of tissues is due largely to changes in hydration levels. [29–31] The spectral response of various tissues in the THz range have no specific spectral features. [14] This is due to the essentially featureless response of water which dominates the response of tissues.

Calculations ranging from hydration levels of 50% to 75% of tissue permittivities show [14] that while the real part of the permittivity does not very much over this range of hydration, the imaginary part varies significantly over the same range. Using a double Debye model (Eq. (4)) to predict the permittivity of water and a Bruggeman effective media theory (Eg.(8)) to predict the permittivity of the tissue, one can calculate the sensitivity of the reflectivity changes (from Fresnel (16)) with respect to changes in hydration. Interestingly, Fig. 4 shows that the sensitivity of the THz reflectivity to water hydration increases in the low (<0.5THz)) range. However, as one decreases the THz frequency to take advantage of the sensitivity, the spatial resolution is reduced due to the increasing THz wavelength. In addition, scattering of THz radiation from

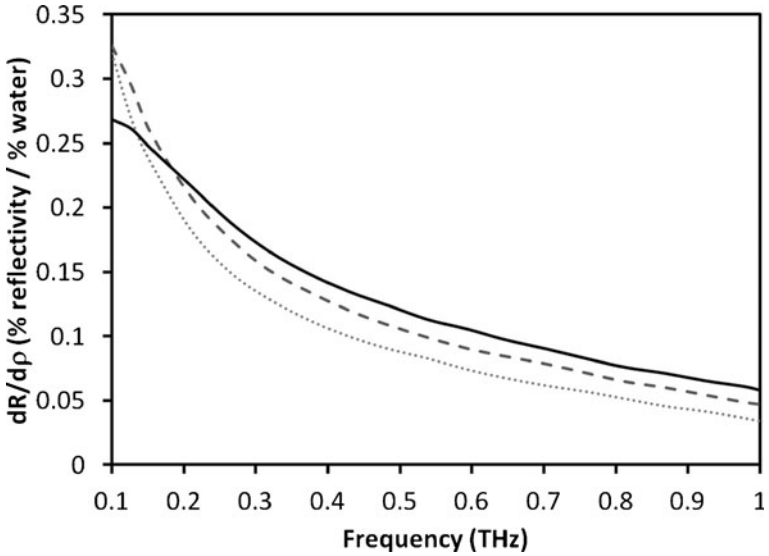

Fig. 4 Hydration sensitivity (change in reflectance per change in water concentration) as a function THz illuminating frequency for 100% *(solid line)*, 75% *(dashed line)* and 50% *(dotted line)* water concentration. Adapted from [14].

rough surfaces of tissues [14] or more generally by the internal structure of a medium (such as the internal structure of leaves [11] and cork [25]) also can affect the optimal frequency. If the size of the roughness or internal structure (pores or holes) in a material were smaller than the wavelength of THz radiation, the scattering would be reduced. As the THz wavelength approaches the same scale as the roughness, enhanced attenuation due to scattering is expected.

Based on the trade-offs among maximized differential reflectance (optimized at low THz frequencies), scattering (minimized at low THz frequencies), and spatial resolution (increasing at high THz frequencies), Talyor *et. al* [14] developed an optimized system for THz Medical imaging operating at 524 GHz with ~125 GHz of bandwidth. The system has a spatial resolution of 1 mm and hydration sensitivities of 0.4% by volume.

Among its many medical applications, THz imaging has been used to study skin burns, melanoma/carcinoma, and hydration levels of cornea. The main issue in burn wound assessment is to determine the penetration depth of the burn into sequential skin layers. Penetration depth refers to the maximum thickness level of skin layers (epidermis tissue and dermis) and deeper hypodermis (subcutaneous) tissue in which burn damage is present. Superficial burns can be treated conservatively while deep partial thickness or full thickness burns require more aggressive medical intervention. [32] The contrast mechanism [33] for THz imaging directly after application of a burn to *ex-vivo* skin samples is the reduction in water content of burned skin compared to normal skin. [14] However, THz studies of *in-vivo* skin burns over time show that the skin's immediate reaction to the burn is a rush of fluid to the burn and surrounding areas. From 1–7 hours post burn, the fluid recedes from the area surrounding the burn and is localized to the burn contact area of the skin. In addition to the pooling of fluid near the burn, other biological effects [34] such as the density of the discrete scattering structures in the skin (such as hair follicles, sweat glands, *etc*.) could play a significant role in the THz response of severe burn wounds.

Terahertz imaging has been shown to differentiate between cancerous and normal skin tissue. As an example, Basal cell carcinoma is a prevalent form of skin cancer and the most common form of cancer worldwide in white populations. Reflected THz pulses from skin tissue [30, 31] can be analyzed to determine the time broadening of the THz pulse. The pulse broadens in time due to the large frequency-dependant absorption of skin tissue. It is observed that Basel cell carcinoma exhibits an increase in THz absorbance compared to normal tissue resulting in THz pulse broadening. It is suggested that the contrast mechanism is due to an increased water content in malignant tissues.

The normal water content of the eye's cornea affects both its transparency and refractive properties. However, many diseases as well as medical procedures such as LASIK eye surgery can perturb the normal hydration levels in the cornea. [14] THz measurements on both corneal phantoms and *ex-vivo* cornea [35] show that the THz reflectivity is strongly correlated with the water concentration level of the cornea. By modeling the corneal tissue in the THz range of frequencies using a Bruggeman effective medium model (Eq. (8)), an approximately linear relationship between THz reflectivity and water concentration is observed.

5 Non-destructive evaluation of forestry products: paper, wood, and cork

5.1 Paper

The moisture content of paper is an important parameter in its fabrication process. The quality of paper is strongly determined by the drying process which requires online monitoring of the moisture content during paper production. [36] Paper properties such as shrinkage and strength are affected by the distribution of moisture. In paper mills, as an example, a major problem is the

tearing of paper due to high moisture content during processing. [37] Non-uniform moisture distributions can lead to a plethora of problems including fracturing in the paper, curling or wrinkling of the paper, and printer misfeeds. Currently implemented moisture technologies in the paper industry [38] do not measure an image of the moisture mapping, but instead record point or averaged measurements.

Dry paper has low THz absorption and scattering. Since paper is mostly comprised of cellulose fibers, it readily absorbs ambient humidity which alters the effective permittivity of the paper. The size of the cellulose fibers are smaller than the THz wavelength justifying that the combination of fibers and absorbed water can be treated as an effective medium. Early measurements on the moisture content of paper using THz used a linear combination of attenuation coefficients for paper and water (Eq. (5)) to model the effective medium. [39]

It has been shown that the moisture content (mass ratio of water to dry paper Eq. (21)) can be empirically determined by measuring the THz attenuation and phase shift as a function of water mass absorbed by paper. Experimental results show a linear change in both THz phase and attenuation with moisture content. [36, 40] The empirical relationship between moisture content and THz attenuation/ phase can be extended by measuring the complex permittivity of the moist paper and using an effective medium model to extract the moisture content.

For example, measurements of the moisture content in paper at 56% ambient humidity show that the increase in the effective refractive index and attenuation coefficient of paper is well modeled using the Clausius-Mossotti equation as an effective medium model. If one were to use a Clausius-Mossotti model and assume that the polarizability is due to spherical particles, one would derive the Maxwell-Garnett equation. Using the Clausius-Mossotti equation in combination with the measured permittivities of 'free' water and dry paper, [41] shows good agreement between the experimental data and a theoretical fit for paper with 1.7% weight liquid water.

A more detailed compositional analysis of moist paper based on the optical properties of dry paper and water using the Bruggeman effective medium model has been reported [42] in which a heterogenous mixture of dry paper content and 'pure' water is assumed. The permittivity of dry paper is measured using THz time-domain techniques, while the permittivity of water is assumed to follow the Double Debye model (Eq. (4)). The measurements are calibrated by recording the THz transmission of paper samples which have been thermograviometrically measured. The thermogravimetric method involves weighing the 'wet' material relative to the dried material after the sample has been heated to drive off any water. The moisture content as a weight percent can then be calculated from

$$Wt\% = 100\% \times \frac{W_w - W_d}{W_d} \tag{21}$$

where the subscripts w and d refer to the 'wet' and 'dry' weights. For thermogravimetric measurements it is also common to measure the physical dimensions of the sample, since swelling of the material often occurs as it absorbs water. Following the analysis of Eq. (15), the measured time-domain transmission waveform is fit to the theoretically predicted waveforms to extract the thickness and moisture content of the paper. The precision in the measured thickness and water content of paper using THz methods is comparable to exiting online sensor technologies in the paper industry.

5.2 Wood

Several groups have suggested to detect the presence of moisture in wood using THz radiation. Fujii *et. al.* [43, 44] demonstrated that millimeter waves near 100 GHz penetrate at most 18 mm into wood enabling inspection for evidence of termite damage. [44, 45] The

measured THz absorbance in wood varies linearly with water content [46]. The monitoring of moisture is wood timbers is an important parameter in the manufacturing process. While low levels of moisture in timbers can improve the material's mechanical strength during the drying process, excess moisture will accelerate the wood's degradation.

As an example of moisture mapping in wood, Fig. 5 shows the concentration of water immediately after liquid is injected into a 14.2 mm thick sample of spruce. As the sample dries, the volume of water is greatly reduced. In comparing the changing false colors (corresponding to THz transmission amplitude) in Fig. 5a and c near the location of water injection, it is clear that concentration of water gradually decreases as one moves away from the point of injection into the bulk of the sample.

5.3 Natural cork

Terahertz (THz) spectroscopy and imaging has been employed as a non-destructive evaluation tool of natural cork enclosures. [13, 25] Natural cork, a product from the Cork Oak (Quercus suber), is utilized in a variety of products including cork stoppers for wine and other beverages. As an enclosure for liquids, it has the desirable properties of being largely impermeable to liquids and gases, as well as compressible. [47] Natural cork stoppers are manufactured such that the long axis of the cork corresponds to the axial direction of cork tree growth whereas the circular cross-section includes both the radial growth direction and the tangential growth direction which is parallel to the grain in the cork. The diffusion of water in natural corks is anisotropic [47] in the radial, axial and tangential directions. It is well-known [47, 48] that the diffusion coefficient in the radial growth direction is larger than that of the other two directions due to the presence of lenticular channels (pores) that run parallel to the radial growth direction. The lenticular channels enable water and gases to diffuse through the cork. In addition, one would expect the presence of cracks, voids, and defects to increase the diffusion. The presence of these potentially highly anisotropic features in the cork implies a highly variable *local* diffusion rate. The extraction and migration of volatile chemicals from the cork [49] will depend on the local diffusion rates and the presence of volatiles in the area of contact between the wine and the cork.

The THz absorbance of both the dry and moisture laden cork can be modeled using the effective medium theories described in Section 2. For dry natural cork, the host material is itself an effective medium material comprised of cell walls with the embedded particles being the cell lumen (ie. empty space inside of the cell walls). Typically, uncompressed cork

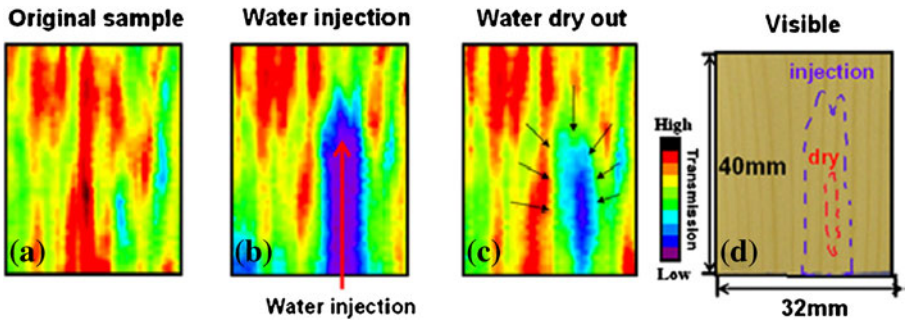

Fig. 5 (**a**) THz transmission image of spruce wood sample. (**b**) Same sample after localized injection of water. (**c**) THz image after sample loses 90% of injected water by weight. (**d**) Visible image of sample. Reprinted from [46], © 2009, with permission from Elsevier.

cells are 80-95% empty space. The Maxwell-Garnett theory was chosen in [13, 25] as the effective medium model for corks.

In the absence of water, the contrast mechanism in the dry cork is predominately due to scattering of the THz radiation by the edges of voids, lenticles, and defects in the cork [25] (Fig. 6). THz absorbance images taken over time as the water permeates the cork disk structure are shown in Fig. 7. In order to create images which only show the flow of water through the cork, the dry cork image is subtracted from each time image leaving only an image representing the absorbance of the water inside the cork. The cork sample in Fig. 7 is oriented so that the radial direction of cork growth is parallel to the bottom of the page. The tangential growth direction is perpendicular to the bottom of the page. Note that while the cork sample is circularly shaped, the diffusion of water does not exhibit radial symmetry due to the varying diffusion rates in the different growth directions. Clearly, the diffusion of water is more rapid in the radial direction of tree growth compared to the tangential direction. It is also clear in comparing Figs. 6 and 7 that the lenticels and cracks/ voids quickly fill with water thereby dominating the diffusion of water.

The average diffusion coefficient of the cork can be extracted from the THz images. Using the data of Fig. 7, the ratio of the water weight content relative to the saturated value M/M_∞ (Eq. (20)) averaged over the entire cork versus time can be calculated. The absorbance fraction is converted to a % weight fraction of water using a measured calibration curve. A best fit using Eq. (20) yields an effective diffusion coefficient of 1.8×10^{-11} m^2/s. A similar analysis of the axial diffusion [13] through cork yields an effective axial diffusion coefficient roughly a factor of 7 smaller than that calculated for the circular cross-section of cork. This result is qualitatively consistent with the immersion measurements of Rosa and Fortes [48] who show that non-radial diffusion is roughly a factor of 4 smaller than radial diffusion.

While averaging of the THz absorbance data over the entire cork yields an effective diffusion coefficient which is comparable to values measured by other means, THz imaging offers the advantage compared to these other measurement techniques of producing time dependant images of the liquid diffusion through the cork structure. Diffusion throughout the cork is not uniform as can be seen in Fig. 7. The inhomogeneity of the cork (e.g due to cracks, voids, lenticular channels) implies that there will be local variations in the diffusion coefficient.

However, monitoring the progress of water through a material using THz imaging may not necessarily be required to extract the material's diffusion properties. For materials such as natural cork in which the contrast mechanism in the images is due to high THz absorbance

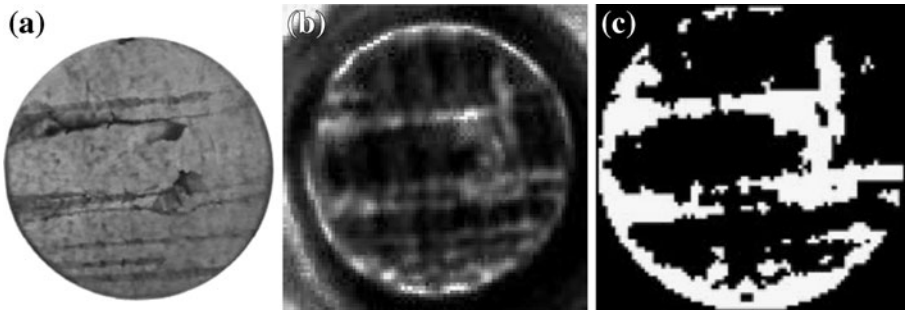

Fig. 6 (**a**) Visible image of 4 mm thick cork disk (**b**) Corresponding THz absorbance image. Bright areas correspond to high THz absorbance. Note high THz absorbance of lenticles and voids in the cork. (**c**) Diffusion coefficient map based on a two value diffusion model corresponding to "high" diffusion (*white*) resulting from lenticles, voids, and cracks in the cork and low diffusion (*black*) in regions of intact cork. Reprinted from [13], © 2011 Springer.

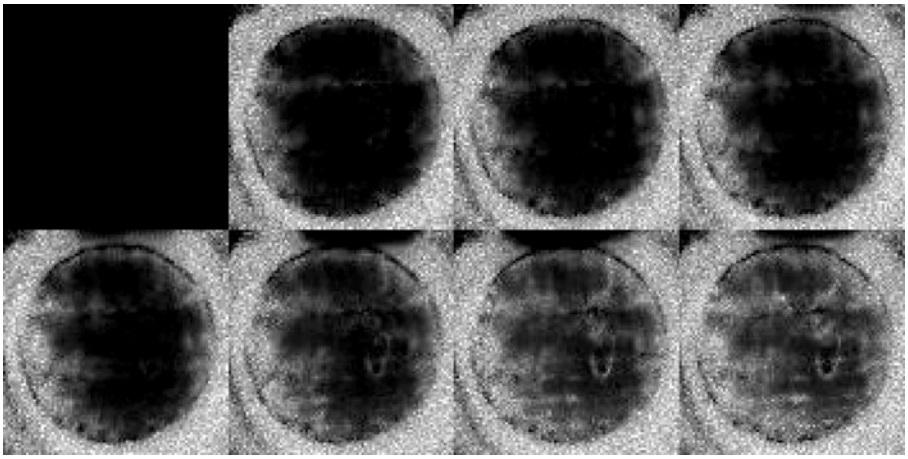

Fig. 7 THz absorbance (0.65–0.7 THz) with dry cork image subtracted at 0 hr (dry cork), 10.9 hr, 21.9 hr, 33 hr, 44 hr, 55.6 hr, 78.2 hr, and 93.6 hr, respectively. Dark regions correspond to low absorbance while bright regions correspond to high absorbance. Reprinted from [13], © 2011 Springer.

enhanced by the scattering of cracks, voids, and defects [25] in an otherwise isotropic material, an image of the enhanced absorbance due to scattering in the *dry* material can indicate locations of high water diffusion in the *wet* material. Since the diffusion of water preferentially tends to follow the channels formed by the cracks, voids, and defects, a dry THz absorbance image – which detects those internal structures - can be used to predict the diffusion of water through the material.

As an example, the dry THz cork image of (Fig. 6) is used to create a map of the local diffusion coefficient. A two-value diffusion model is used. For THz absorbance of the dry image above a fixed threshold, the diffusion coefficient is assumed to be high. For THz absorbance below the threshold, the diffusion coefficient is assumed to be 15 times smaller. These two values are also constrained so that the average diffusion coefficient for the cork must be consistent with the value extracted from Eq. (20). Using the two value diffusion coefficient map, Eq. (17) is numerically integrated in time at each pixel position to calculate the updated water concentration map in time. The resulting water concentration map at 44 hours is shown in Fig. 8. While there are differences in comparing the experimental and predicted diffusion wavefront images at 44 hr, the simple two-value diffusion map creates a diffusion wavefront which resembles the measured wavefront: The more rapid encroachment of water from the left and right compared to top and bottom indicates an anisotropic diffusion coefficient and a larger diffusion coefficient along the lenticular channels. Moreover, this comparison illustrates the potential for using THz imaging of dry images – resulting from the contrast in the THz image due to lenticels, cracks, voids, and defects – to predict the diffusion of water in natural cork structures.

6 Plastics and wood composites

It is widely known that the electrical, physical and mechanical properties of polymers can be greatly influenced by their water content. For example the hydroscopicity of polymer and copolymer materials has been characterized to identify optimal polymers for THz optical components. [50] Similar studies have been performed on polyimide, [51] which is widely

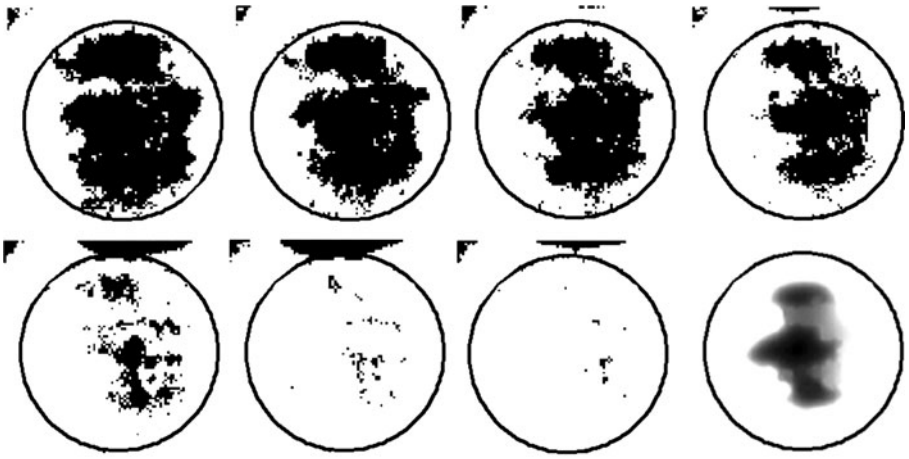

Fig. 8 Tracking of the diffusion front using a 0.5 absorbance threshold at 10.9 hr, 21.9 hr, 33 hr, 44 hr, 55.6 hr, 78.2 hr, and 93.6 hr, respectively from left to right, top to bottom. The large circle indicates the location of the sample. The bottom right image the predicted diffusion front at 44 hrs based on a diffusion map from the dry THz image. Note the similarity of the predicted diffusion wave front to the experimentally measured front at 44 hrs. Reprinted from [13], © 2011 Springer.

used as a packaging material for electronic devices. The structural integrity of composite materials is strongly affected by moisture. Composites with woven fiber reinforcement degrade and the bonding strength of the fiber-matrix interface weakens due to plasticization and swelling of the polymer matrix [52] in the presence of moisture. Wood-Plastic composites, which are widely employed in construction applications, likewise experience a degradation of their physical or mechanical properties due to water penetration. [12]

There have been extensive studies which detail THz imaging to measure the water content in hygroscopic polymers and components such as polyamide and wood plastic composite. [8, 12] Similar to hydration studies of leaves (Section 7.1), thermogravimetric measurements (Eq. (21)) and effective medium models (Section 2.3) of polymers and wood-plastic components need to take in to account the swelling of samples with hydration. For example, the volume fraction of water, can be expressed [12] as

$$X_w = \frac{m_w - m_d}{\rho V} \tag{22}$$

where ρ, V, m_w, and m_d are the mass per unit volume of water, the measured sample volume (including swelling), the measured mass of the wet material, and the measured mass of the dry material. Moreover, as the polymers absorb water, the water can be in the form of 'free' or 'bound' water (Section 2.2). The interactions of the water with the host material change the vibrations of the bound water relative to the free water resulting in a slightly different permittivity response. For high water content typically above the fiber saturation limit, one can expect free water to collect in the 'voids' of a material. Wood-Polymer composites have a fibre saturation point after which free water is stored in the voids of the composite structure. In addition to polymer and wood-plastic composites, natural cork (Section 5.3) also has this property: The lumens of the cork cells in the cork will fill after the walls of the cell are saturated, typically at roughly 60% water weight. [47] As long as one is well below the saturation point, it can be reasonably assumed that the only bound water is present in the host material structure.

For the polymer composites, there are three components to the effective permittivity: the permittivity of 'solid' polymer, the permittivity of air (voids and lumens), and the permittivity of bound/free water. Unlike dried compressible materials, such as leaves, which can be compressed to remove the air thereby enabling the independent THz spectroscopy measurement of 'solid' host material (Section 7.1), polymers are not so easily compressed to remove the trapped air. There have been two different approaches to including the voids and lumens into the 'solid' host material using an effective medium model. The first approach [12] is to treat the combined polymer/ void/lumen system as one 'host' material. As this 'host' material absorbs water, the volume fraction of water increases, but the optical properties of the 'host' material change since the empty space is replaced by water. The approach of [12] is to account for the replacement of empty space by water in the 'host' material by defining an effective refractive index of the dry polymer host which changes as the volume fraction of empty spaces changes:

$$n_{PD}(t) = \frac{[n_{PD}(t_0) - 1]d_o}{X_{PD}(t)d(t)} + 1 \tag{23}$$

In the above equation, d_o and $n_{pD}(t_o)$ are the dry sample thickness and refractive index of the plastic/void/lumuns before water is absorbed, while $X_{PD}(t)$ and d(t) are the volume fraction of the dry polymer and the sample thickness at some later time as water is absorbed. Essentially, Eq. (23) is an 'effective medium' model to account for the loss of empty space within the polymer/void/lumen host material.

The second approach as applied to natural cork [13] is to treat the dry cork itself as an effective medium consisting of a host material of solid cell wall material (or solid polymer in analogy with [12]) embedded with isolated void pockets. Estimating the volume fraction of air in the dry cork allows one to calculate the permittivity of 'solid' cork cell walls. The effective permittivity of the wet cork is calculated using subsequent applications of the Maxwell-Garnet effective medium approximation to water absorption by the 'solid' cork cell material plus the remaining air 'particles'.

From the THz transmission data, one can use Eq. (15) to calculate the refractive index and absorbance of a "slab" of the effective material. With the measured permittivity values for the dry polymer, Equations (3), (4), (12) and (23) can be used to extract the volume percent of water in the material. The measured real refractive index and absorption coefficient of polyamide, with this approach, are shown [12] to increase approximately linearly as a function of water content for samples with up to 10% water by weight.

Based on the results presented above, a terahertz time-domain system has been developed for inline process monitoring of the plastics extrusion process. [53] As part of the online capability, the moisture content of the polymers can be monitored. As one would expect based on the discussions in Section 2, as the water content increases, there is a larger relative impact of water on the effective permittivity of the hydrated polymer leading to an increase in both the real refractive index and absorption coefficient of the polymer. These results suggest that THz transmission measurements can be utilized as a non-destruction evaluation method for measuring the water content in hygroscopic plastics and related compounds.

7 Agriculture – leaves, crop yield, pecans, wheat, food inspection

7.1 Drought stress monitoring through leaf water content

Measuring the moisture content of leaves was one of the first applications of THz imaging and sensing. As mentioned in the introduction, the first THz time-domain image was taken

of a drying leave [5] while one of the early applications of THz sensing was to monitor the moisture level of tobacco products. [7] More recently, moisture monitoring of plants through the water content of their leaves has emerged as an important application of THz technology. Evaluation of leaf water content provides valuable information to farmers and scientists concerning plant drought stress and irrigation management. With limited water resources in some regions of the world, optimal use of available water and efficient irrigation become critical issues. A major metric for optimizing irrigation strategies is to recognize drought stress of plants in the field. One possible solution is to monitor the drought stress of plants through the hydration levels in leaves via THz techniques. Consequently, physiological studies of a leaf's hydration state and underlying water transport mechanisms of plants are important. [8] In their 1996 review article on THz imaging, Mittleman *et. al* claimed [6] that "currently, there is no accepted, nondestructive procedure for measuring the leaf water status of a transpiring plant."

As shown in data from [8], there is a linearly decreasing THz transmission with water content in leaves. Early measurements from Mittleman [6] demonstrated the potential for measuring the time dynamics of water transport in a leaf (Fig. 9). For this measurement a house plant was exposed to mild drought stress so that the plant cells were not at full turgor (meaning that the plant cells would allow water entry into the cells). After watering the plant and some time delay, the decrease in THz transmission across the leaf indicates the flow of water into the leaf's structure.

As this application has evolved, several papers have focused on accurate measurements of the leaf's hydration level by modeling the complex permittivity of leaves in the THz frequency range. By modeling the complex permittivity of coffee leaves, it has been demonstrated that the dielectric properties of the leaf can be utilized to determine the water content of the leaves and hence monitor drought stress in the plant. [11] One complication in modeling the hydration of leaves (as well paper and natural cork) is that the measured leaf thickness changes with hydration and is correlated with the volumetric water content of the

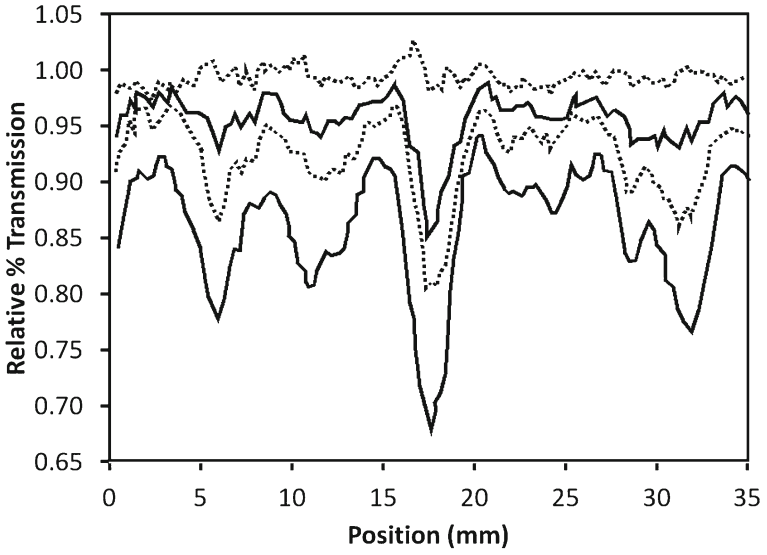

Fig. 9 Terahertz scan along a line which bisects the center of a leaf adapted from [6]. The modulation (localized decrease in transmission) for each line scan is indicative of the leaf's stem structure. Traces from top to bottom correspond to 10, 60, 190, and 470 minutes after watering.

leaf. [11, 54] Consequently, one typically needs to extract both the sample thickness and complex permittivity simultaneously through data analysis.

To extract accurate measurements of the hydration level, a leaf was considered to be comprised of three components: water, air, and solid plant material. [11] As the hydration level in a leaf varies, the relative volume fraction of the constituents change. The volume fraction of plant material is calculated by drying a sample of leaves and then compressing them to remove all air. THz transmission measurements of the dried/ pressed leaves was used to measure the permittivity of solid leaf material. The Double Debye formula (Eq. (4)) is used to model the permittivity of water. The volume fraction of the plant material is the ratio of the sample thickness after drying/pressing relative to the thickness before drying. The volume fractions of air, water, and solid plant material is determined by the equation $X_\alpha+X_w+X_s=1$.

Jordens *et. al* [11] use the Looyenga model for the water, solid leaf material, and air effective medium since that model can characterize irregularly-shaped particles. While they achieve good agreement with the real refractive index, there is a large discrepancy between the predicted and measured absorption of the leaf. When scattering by the effective medium is included through a Rayleigh roughness factor (Eqs. (13)-(14)), there is excellent agreement between the measured and predicted THz absorbance, transmission, as well as volumetric water content (Fig. 10). For this measurement a particular leaf of the coffee plant is measured over time. The volumetric water content in Fig. 10 is calculated from the measured permittivity (accounting for surface scattering) of the leaf as described above. The data is fit to an exponential decay which is then use to calculate the expected transmission based on a calibration between volumetric water content and THz transmission. Note the excellent agreement between the measured and calculated THz transmission indicating that the inferred water content of the leaf is self-consistent.

Other groups have inferred the water content of a leaf without extracting the effective permittivity. Using a continuous wave source at 0.189 THz, [55] measured the THz transmission image through a drying spinach leaf. Time-dependant images of the relative water concentration are calculated by subtracting at each pixel the background absorbance of the dry leaf from the THz absorbance of the wet leaf. Since the 'background' absorbance of the dry leaf is subtracted from each image, the net absorbance at each pixel in the image is proportional to the concentration of water. The absorbance images are calibrated assuming that the Beer-Lambert absorbance law is obeyed.

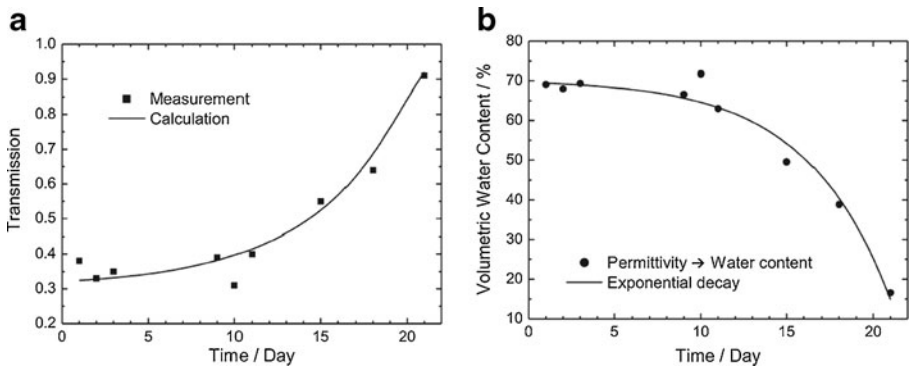

Fig. 10 Transmitted THz intensity (**a**) and volumetric water content (**b**) of coffee leaf subject to drought dress. Reprinted from [11], © 2009, Springer.

Hadjiloucas *et. al* [54, 56] illustrate another example of inferring a leaf's water content without extracting the effective permittivity. Using a principle component analysis, Hadjiloucas *et. al* show their THz spectroscopy data could be used to extract water leaf content [57] resulting in significant differentiation between wet, dry (~60% water content of wet leaf) and oven dry leaves. In analogy with infrared (IR) multispectral measurements for determining water content of leaves by satellite imaging, Hadjiloucas *et. al* [58] extend their laboratory experimental concept to consider measuring water content by airborne imaging with THz radiation. While that paper does not consider the affect of atmospheric attenuation on the probing THz radiation (which is well-known to be problematic for stand-off THz detection [1]), they develop in analogy with IR imaging a water content index (WCI) in the THz range given by

$$WCI_{THz} = \frac{-\ln[1 - R(\nu_1) - R(\nu_2)]}{-\ln[1 - R_{ft}(\nu_1) - R_{ft}(\nu_2)]} \tag{24}$$

where the subscripts *1* and *2* refer to the two THz frequencies at which the reflectivity is measured, and the subscript *ft* refers to measurements of reflectivity made at full turgor, meaning that the plant cells are full of water and resist further water entry into the cell. Hadjiloucas *et. al* argue [58] that a THz based system for extracting water content should be superior to an IR based system because the absorbance lines of water at THz frequencies are stronger than in the IR band. In addition, the precision could improve by choosing one THz frequency for which there is strong absorption due to water while the second is only weakly absorbed by water.

The appropriate wavelengths for the WCI definition can be chosen with the aid of Fig. 4, which shows the expected sensitivity in reflectivity due to changes in hydration level for a model system. One factor is clear from this plot: all THz frequencies (up to 1THz) exhibit a change in reflectivity with moisture due to the essentially featureless spectral absorbance of water in the THz range. Therefore, to optimize the proposed WCI in the THz range, the "strong" THz absorbance frequency should be chosen to be near 100 GHz, while the "weak" absorbance peak should be ≥1 THz. Of course the choice of wavelengths needs to consider the atmospheric transmission windows in the THz range.

7.2 Dried food

The moisture content in dried food can be monitored using THz techniques. [59] The moisture affects food quality properties including taste, texture, mechanical strength, bacterial growth, and shelf-life. [60] While water strongly absorbs terahertz radiation, other constituents such as proteins typically exhibit absorption coefficients 100 times smaller than water. Fats and lipids are typically 20 times less absorptive than water, while starch is roughly 50 times lower absorbance than water in the THz range. A quantitative demonstration of moisture measurements in dried food was performed by Parasoglou *et al.* [61, 62] In that work, the samples were starch wafers which are commonly used in the confectionary food industry. The wafers exhibit low moisture content and porous structure. As discussed in [62], THz measurements are dominated by absorption due to moisture content, assuming that scattering due to holes or pores in the food is small. The THz absorbance is then relatively immune to small fluctuations in the concentration of other constituents of the food sample since the relative absorbance of water is so much higher than the other constituents. Another advantage of using THz measurements is that the minimal THz power does not result in any significant heating of the sample. Parasoglou *et. al* measured a linear relationship between the moisture content in the wafers and

the normalized peak-to-peak amplitude of the THz time-domain pulse. When the data is analyzed in the frequency domain, there is a linear relationship between the transmission amplitude and moisture content in the region between 0.2-0.6THz. Above 0.6THz, the attenuation of the THz signal is dominated by scattering of pores in the food wafer rather than by the presence of moisture. A complete analysis of the measured THz absorbance would require the inclusion of scattering (Eqs.(13)-(14)).

7.3 Quality control of Pecans

The prospect of using THz imaging as a non-destructive evaluation technique for pecan nuts has been explored. [63] Since the water content of the nutmeats inside of the shell are low, the pecan nuts are fairly transparent to THz radiation. Therefore, enhanced THz absorbance may indicate the presence of a defective product. One common defect in pecans is the presence of living insects which feed on the nutmeat. Since living insects usually contain 70-80% water while the water content of nutmeats are typically less than 10%, THz absorbance based on the presence of water could be used to identify product contamination by insects which are feeding on the interior nutmeat.

7.4 Moisture content of crushed wheat grain

THz technology was used to measure the moisture content of crushed wheat grain. [64] As discussed in [64], grain process engineering requires advanced sensory systems to measure the moisture content and moisture distribution in grain kernels and crushed wheat in order to optimally control grain processing and storage. Wheat grain is typically stored at 8-10% moisture content to prevent germination. Milling requires the moisture content of the wheat to increase to 16.5%. A non-uniform moisture distribution in the grain causes problems with milling. Experimental measurements on crushed grain show a linearly decreasing THz transmission with increasing humidity levels up to 18%.

7.5 Quality control of damaged fruit

The prospect of using THz imaging to assess the damage to tomatoes caused by pressure on the outer surface of the fruit has been explored. [65] The pressure damages the fruit cell walls which causes a local filling with water. Over time, the damaged area looses moisture resulting in a brownish color to the fruit surface. Measurements on damaged tomatoes show a decrease in THz reflectivity from regions where were slightly pressed. Unfortunately, a detailed analysis of the change in permittivity was not discussed. The authors proposed that the decrease in reflection resulted from the increase in absorbance by water which fills the damaged area. As shown in Fig. 4, however, when one considers the effective permittivity of a medium, an increase in water content should lead to an increase rather than a decrease in reflectance. Another effect which complicates the reflectance measurement is the fact that the surface of the tomato is curved, which leads not only to a Gouy phase shift in reflection, [66] but also the need to treat the curvature and changes in curvature of the fruit as an effective curved mirror in the optical analysis of the THz reflection system.

7.6 THz imaging for crop yield estimates

In this section, a novel application of pulsed THz imaging for moisture detection is described. The concept is to use the high reflectivity of water to identify and ‘count’ high

water content fruit and/or vegetables which are hidden behind a canopy of leaves. [66] THz imaging for crop yield estimation has the seemingly contradictory requirements to penetration through a thin layer of fairly high water content (ie. the leaves) and then reflect from a second region of high water content (the fruit). The potential advantage of THz imaging compared to other methods of crop yield estimation is the ability of THz radiation to penetrate through a thin canopy *in-situ*. As described in Section 7.1, the water content in the leaves attenuate THz radiation. However, grape leaves transmit roughly 25% of the THz power at 200 GHz. Using a pulsed THz imaging system to acquire the images, the reflection from the leaf can be separated from the THz image of the fruit by choosing a time window which excludes the direct reflection from the leaf.

Remote sensing utilizing satellite or airborne imaging in several spectral bands has been applied to agriculture monitoring. Typically by examining the difference in light reflection at two or more visible or near-infrared spectral bands, estimations of foliage health can be used to estimate the crop yield. For example, the Normalized Difference Vegetation Index (NDVI) uses spectral data from 580-680 nm (corresponding to absorption from chlorophyll) and 725-1100 nm (corresponding to high reflectance from the leaf structure) to create images of plant growth, vegetation cover and biomass production. In the case of crop estimation in vineyards, there is not a good correlation between multispectral satellite imaging and the crop yield; grape vines may be pruned several times in a growing season so that there is no strict correlation between the 'greenness' of the foliage or canopy size and yield. Moreover, since the grape clusters are typically partially covered by the canopy, direct visible imaging of the grape berries is difficult.

Estimation of grape yield includes three factors: clusters per vine, berries per cluster, and berry weight. Due to the high water content of the grape berries, THz imaging can detect the presence of berries enabling a measure of the number of clusters per vine. The number of berries per cluster can also be estimated by using sufficiently high THz frequencies so that individual berries can be identified in a THz image (although there is still a "shadowing" effect of one berry hidden behind another). One can also possibly estimate the berry weight, although the estimate would be indirect. In essence, the size of the berry can be estimated from THz images and the weight of the berry can be inferred by knowing that there is a strong correlation between the berry's size and weight. [67]

Analysis of the reflected time-domain THz pulses show that the high water content and surface curvature of the grape berries produce a Gouy phase shift [66, 68, 69] in the reflected THz pulse which enables differentiation among the various grape vine components. Gouy phase shift refers to a longitudinal phase shift of a Gaussian beam as it passes through its focus. The Gouy phase shift is in addition to the normal change in phase as the beam propagates. The essential concept is that the curved surface of the fruit is part of the optical system which affects the phase and amplitude of the reflected THz beam. Figure 11a shows a comparison between typical time domain waveforms from a berry, leaf, stem, and reference flat gold mirror. Clearly the berry's phase appears to be shifted with respect to the others. Figure 11b shows the measured reflected THz waveform from a berry as well as the predicted waveform based on the anticipated Gouy phase shift [66]. When the Gouy phase correction is included there is excellent agreement between the measured and predicted waveform.

The potential of utilizing this methodology for agriculture crop yield estimates has been explored by following the development of grape clusters from the formation of berry flowers through harvest. The Gouy phase shift differentiation occurs early in the growing season while there is little foliage on the grape vines and continues until harvest. Tests were conducted to eliminate the possibility that details of the berry structure were responsible. If the skin of the berries were removed, similar THz waveforms and phase shifts are measured. Similar results have been obtained with a variety of thin-skinned, high water

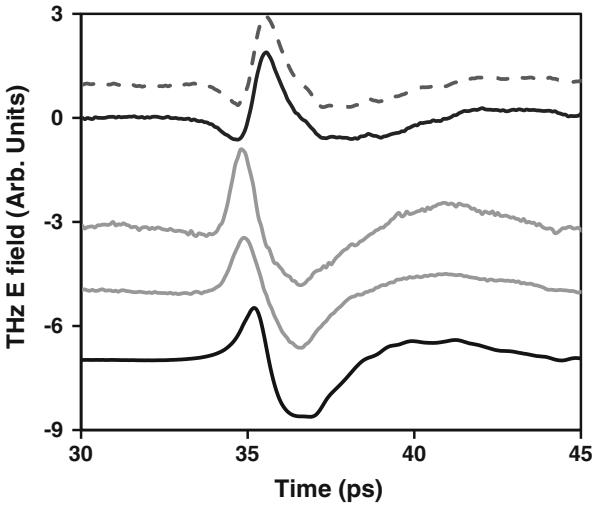

Fig. 11 Comparison of THz time-domain reflectance waveforms from the reference, leaf, stem, berry, and predicted waveform including the -π/2 Gouy phase shift (bottom to top). The predicted waveform with the Gouy phase shift accurately reproduces the measured waveform from the berry. Adapted from [66].

content fruit such as blueberries, cherries, and plums suggesting that the pulsed THz imaging method can be used to differentiate these fruits from the leaves and stems as well.

8 Other applications

8.1 Paint and art preservation

In the past few years, THz imaging has found an innovative application to art preservation and the non-destructive evaluation of paints. In regards to moisture (or more generally solvent) detection, THz techniques have been adapted to monitor the drying of applied paint. [70, 71] When a paint layer is deposited and monitored using a pulsed THz system, there is a time delay between the THz pulse which is reflected by the air/paint interface and the pulse reflected by the paint/ substrate interface. By monitoring the time evolution of the composite THz reflected pulse, one can observe the overlap between pulses reflected from the air/paint and the paint/substrate boundaries. Over time as the solvent evaporates, the paint layer shrinks and the overlap of the reflected pulses increases. Eventually, the evolution of the reflected THz pulse waveform ceases indicating that the paint has dried. For art conservation, THz imaging could be used to monitor the water content distribution in paint layers or plasters during cleaning or consolidation processes. [72] It has also been suggested that THz can be used to detect water content or damage in artifacts and artwork. [73]

8.2 Concrete

There have been only a few studies of the moisture content in concrete using THz techniques. In one study, THz sensing was used as a non-destructive method for evaluating moisture content of concrete structures [74]. In hardened cement paste, there are two general types of water present: water which is chemically bound as part of the concrete mixture and volumetric water which can be removed by evaporation. The goal of [74] was to select the appropriate THz frequency to identify the presence of volumetric water without being sensitive to chemically bonded water. At a frequency of 0.05THz, a linear relationship

between the volumetric water and THz transmission is observed. At higher frequencies, the THz transmission appears to be affected by the presence of the chemically bound water.

In another study, Oyama *et. al* [46] demonstrated the ability of THz imaging to detect the preferential diffusion of water along cracks in concrete. Their work is motivated by the desire to monitor the mechanical strength of concrete, which depends on hydrate formation between cement and aggregates. The mechanical strength of concrete can be weakened by a de-alkaline chemical reaction. This reaction depends on the diffusion of water into concrete blocks as well as the presence of salts in the aggregates. Conceptually, one could potentially monitor the mechanical strength and degradation of concrete if one could utilize THz imaging to measure the water content and monitor the diffusion of water through concrete. Using a THz imaging system, they demonstrate the preferential diffusion of water along the cracks. However, they do not estimate the overall water content of the concrete, nor the volume of the crack, nor the diffusion rate of water. From Oyama *et. al*'s prospective, they view the detection of water in concrete as a mechanism to enhance the sensitivity of non-invasive crack detection in concrete using the high dielectric contrast between water and concrete in the THz range. Based on the proportionality of volumetric water to THz transmission [74] as well as the ability of THz imaging to detect cracks and voids in materials, non-destructive monitoring of the mechanical strength of concrete may be a worthwhile application of THz moisture sensing, but further development of the technique is required.

9 Conclusion

Moisture detection and mapping using Terahertz techniques is reviewed. The predominate contrast mechanism in the THz region results from the large permittivity difference between liquid water and other constituents in samples. While this review focuses mostly on moisture, clearly the same principles can be applied to the detection and diffusion mapping of other liquids as long as the permittivity of the liquid is much higher than that of the surrounding materials. Beginning with qualitative observations noting the variation in THz transmission with the 'dryness' of a host material, the application of THz techniques has evolved to the extraction of localized moisture levels through the analysis of moist materials as an effective medium. Effective medium models are used to integrate the individual permittivities from water, air, and 'dry' constituents into an effective permittivity of the 'wet' material. The goal of the effective medium analysis is to use the measured THz transmission or reflection from the effective medium to extract the volume fraction of water.

THz imaging is shown to be a viable non-destructive evaluation tool not only for point measurements of water content, but also as a tool to visualize the spatial dependence of moisture. Typical time-scales for water diffusion in materials are on the order of hours or days. Since state-of-the-art THz imaging systems can scan objects in much shorter time periods (typically a few to tens of seconds), the speed of THz imaging hardware is not a critical issue for 2-D diffusion or moisture mapping. Typical spatial resolutions for ~1THZ radiation are limited by diffraction effects to ~300 μm which enables one to image water diffusion into comparably-sized cracks and voids in concrete, natural cork, composite plastics, and other materials. While the presence of small cracks in materials may not create a large contrast in 'dry' THz absorbance images, the penetration of a liquid with high permittivity into those cracks will produce an enhanced contrast in 'wet' THz absorbance images. THz images can be analyzed to extract the spatial topology of a water diffusion wavefront, the local hydration level, and the average diffusion coefficient. THz imaging easily enables one to visualize the anisotropic and locally varying diffusion coefficient.

While the various applications of THz sensing to moisture detection show great potential, there are still scientific and technological issues to be addressed. For example in moisture laden materials, the differentiation between bound and free water could be a primary concern. However, the problem of differentiating bound from free water using THz spectroscopy is a complex problem without a simple methodology to experimentally separate the respective contribution to the effective dielectric. There is an open question for any particular material as to which is the best effective medium model to employ. For example, some are best applied in the limit of small value fractions of particles, while others for particles which exhibit particular shapes. Symmetric models effectively treat the host and particle materials as exchangeable components, while asymmetric models recognize that the polarizability of an effective medium as a function of the particle's volume fraction would change if the role of host and particle were exchanged. For given volume fractions and permittivities for the host and particle material, the choice of a particular effective medium model can significantly alter the predicted effective dielectric of the medium. The approach taken by some researchers is to choose the effective medium model which best predicts the measured THz transmission or reflection data over a wide range of moisture content.

Medical applications of THz moisture sensing have shown significant potential for diagnosis of skin cancer, burns, and moisture levels in eye corneas. Due to the THz reflection geometry inherently required for medical sensing, one must find a balance between sensitivity of the THz reflectivity to moisture changes (which increases at low THz frequencies), increased spatial resolution (at higher THz frequencies), and frequency dependant THz scattering. In the future, one would expect that the potential shown in *ex-vivo* measurements (for burns and corneas) will be demonstrated with *in-vivo* use on patients.

Industrial as well as agriculture applications of THz moisture sensing have shown tremendous potential in the laboratory but adaptation in industrial processes has not been extensive. For applications in which there have been a significant number of papers (*e.g.* leaves, paper, plastic composites, and natural cork), the needs and industrial requirements have been clearly identified, but the adaptation of the THz technology into the industrial processes has not been widespread to date. Other applications have shown some potential (*e.g*. concrete and quality control of damaged fruit), but more effort must be spend on developing these application in order to effectively demonstrate the capabilities of THz sensing. For example, THz images of water diffusing through concrete need to be analyzed to measure diffusion coefficients, the volume of water in the cracks and defects, and lastly show a correlation between the THz moisture images with the presumed mechanical weaknesses which develop in the structure. The application of THz moisture imaging to damaged fruit needs to incorporate effective medium models so that the effective dielectric of the fruit can be extracted and correlated with damage to the fruit.

While there are many papers and examples concerning the detection of moisture in materials including THz absorbance images which can be correlated to spatial maps of the local water content, there have been relatively few papers which analyze the time evolution of the water content images to extract either an average or local diffusion coefficient. Clearly, comparison and analysis of time-dependant THz images with numerical solutions to the diffusion equation will be required to (a) extract a map of the anisotropic and inhomogenous diffusion coefficient and (b) determine if *dry* THz images, like those of natural cork, can be used to predict the local diffusion coefficient. To date, there have been no detailed comparisons of the experimentally measured time-progression of liquid diffusion by THz imaging with modeling or simulations of the diffusion process. While examples of water diffusion measurements in 2-D are abundant, water's absorbance is too large to permit 3-D THz imaging of thick, moisture laden samples to be feasible. However, if the THz absorbance of a 'dry' image is dominated by the internal structures of the material, one can

use a THz image of the internal structures as a 3-D map of preferred diffusion pathways. For example, the cracks, voids, fissures, and scratches in materials may represent routes of rapid water diffusion. Based on the presence and organization of these defects, the diffusion of water through the structure can be numerically predicted as if the sample were exposed to water. The use of THz 'dry' 3-D images to predict the moisture diffusion in those materials is the next step in extending THz moisture sensing not only to 3-D structures, but also to demonstrate the potential of characterizing the diffusion of liquid through samples without having to expose the sample to moisture. This could enable non-destructive evaluation of diffusion properties of samples without waiting the hours or days required for typical diffusion processes to occur.

Acknowledgements Helpful discussions with Prof. J. M. Joseph are gratefully acknowledged. The author gratefully acknowledges helpful discussions with H. Grebel and U. Kaatze concerning effective medium models.

References

1. Federici, J.F., *et al*., *THz imaging and sensing for security applications - Explosives, weapons and drugs.* Semiconductor Science and Technology, 2005. **20**(7).
2. Michalopoulou, Z.H., *et al*., *RDX detection with THz spectroscopy.* Journal of Infrared, Millimeter, and Terahertz Waves, 2010. **31**(10): p. 1171–1181.
3. Federici, J. and L. Moeller, *Review of terahertz and subterahertz wireless communications.* Journal of Applied Physics, 2010. **107**(11).
4. Moeller, L., J. Federici, and K. Su, *2.5Gbit/s duobinary signalling with narrow bandwidth 0.625 terahertz source.* Electronics Letters, 2011. **47**(15): p. 856–858.
5. Hu, B.B.N., M C, *Imaging with terahertz waves.* Optics Letters, 1995. **20**(16): p. 1716–1718.
6. Mittleman, D.M., R.H. Jacobsen, and M.C. Nuss, *T-ray imaging.* IEEE Sel. Top. Quantum Electron, 1996. **2**: p. 679–92.
7. Chan, W.L., J. Deibel, and D.M. Mittleman, *Imaging with terahertz radiation.* Rep. Prog. Phys., 2007. **70**: p. 1325–1379.
8. Jansen, C., *et al*., *Terahertz imaging: applications and perspectives.* Appl. Opt., 2010. **49**(19): p. E48-E57.
9. Mittleman, D., *Sensing with terahertz radiation*. Sensing with Terahertz Radiation. 2003.
10. Reid, M. and R. Fedosejevs, *Terahertz birefringence and attenuation properties of wood and paper.* Appl. Opt., 2006. **45**: p. 2766–72.
11. Jördens, C., *et al*., *Evaluation of leaf water status by means of permittivity at terahertz frequencies.* J Biol Phys, 2009. **35**: p. 255–264.
12. Jordens, C., *et al*., *Investigation of the water absorption in polyamide and wood plastic composite by terahertz time-domain spectroscopy.* Polymer Testing, 2010. **29**: p. 209–215.
13. Teti, A.J., *et al*., *Non-Destructive Measurement of Water Diffusion in Natural Cork Enclosures Using Terahertz Spectroscopy and Imaging.* J. Infrared Milli. Terahz. Waves, 2011. **32**: p. 513–527.
14. Taylor, Z.D., *et al*., *THz Medical Imaging: in vivo Hydration Sensing.* IEEE transactions on THz Science and Technology, 2011. **1**(1): p. 201–219.
15. Liebe, H.J., G.A. Hufford, and T. Manabe, *A model for the complex permittivity of water at frequencies below 1 THz.* International Journal of Infrared and Millimeter Waves, 1991. **12**: p. 659–675.
16. Kaatze, U. and C. Hubner, *Electromagnetic Techniques for moisture content determination of materials.* Meas. Sci. Technol., 2010. **21**: p. 0821001.
17. Balakrishnan, J., B.M. Fischer, and D. Abbott, Appl. Opt., 2009. **48**: p. 2262–2266.
18. Maxwell-Garnett, J.C., Phil. Trans. R. SOc. Lond. Ser. A, 1904. **206**: p. 385–420.
19. Choy, T.C., *Effective Medium Theory: Principles and Applications*. International Series of Monographs on Physics. 1999: Oxford.
20. Bandyopadhyay, A., *et al*., *Effects of scattering on THz spectra of granular solids.* International Journal of Infrared and Millimeter Waves, 2007. **28**(11): p. 969–978.
21. Beckmann, P. and A. Spizzichino, *The Scattering of Electromagnetic Waves from Rough Surfaces*. 1987, Norwood: Artech House.

22. Stoik, C., M. Bohn, and J. Blackshire, *Nondestructive evaluation of aircraft composites using reflective terahertz time domain spectroscopy.* NDT and E International, 2010. **43**(2): p. 106–115.
23. Rahani, E.K., *et al*., *Mechanical damage detection in polymer tiles by THz radiation.* IEEE Sensors Journal, 2011. **11**(8): p. 1720–1725.
24. Stoik, C.D., M.J. Bohn, and J.L. Blackshire, *Nondestructive evaluation of aircraft composites using transmissive terahertz time domain spectroscopy.* Optics Express, 2008. **16**(21): p. 17039–17051.
25. Hor, Y.L., J.F. Federici, and R.L. Wample, *Nondestructive evaluation of cork enclosures using terahertz/ millimeter wave spectroscopy and imaging.* Applied Optics, 2008. **47**(1): p. 72–78.
26. Topgaard, D. and O. Soderman, *Diffusion of water absorbed in cellulose fibers studied with 1H-NMR.* Langmuir, 2001. **17**: p. 2694.
27. Obradovic, J., *et al*., *The use of THz time-domain reflection measurements to investigate solvent diffusion in polymers.* Polymer, 2007. **48**: p. 3494–3503.
28. Crank, J., *The Mathematics of Diffusion*. 2001, Oxford: Clarendon.
29. Pickwell, E. and V.P. Wallace, *Biomedical applications of terhertz technology.* J. Phys. D: Applied Physics, 2006. **39**: p. R301-R310.
30. Woodward, R.M., *et al*., *Terahertz pulse imaging in reflection geometry of human skin cancer and skin tissue.* Physics in Medicine and Biology, 2002. **47**(21): p. 3853–3863.
31. Woodward, R.M., *et al*., *Terahertz pulse imaging of ex vivo basal cell carcinoma.* Journal of Investigative Dermatology, 2003. **120**(1): p. 72–78.
32. Jaskille, A.D., *et al*., *Critical review of burn depth assessment techniques: Part I. Historical review.* Journal of Burn Care Research, 2009. **30**: p. 937–947.
33. Suen, J.Y., *et al*., *Towards medical terahertz sensing of skin hydration.* Studies in Health Technology and Informatics 2009. **142**: p. 364–358.
34. Arbab, H., *et al*. *Characterization of burn injuries using terahertz time-domain spectroscopy*. in *Progress in Biomedical Optics and Imaging - Proceedings of SPIE*. 2011.
35. Bennett, D.B., *et al*., *Terahertz sensing in corneal tissues.* Journal of Biomedical Optics, 2010. **16**(8): p. 8.
36. Banerjee, D., *et al*., *Diagnosing water content in paper by terahertz radiation.* Opt. Express 2008. **16**: p. 9060.
37. Carts-Powell, Y., *Terahertz imaging brings new capabilities to QC applications*. Laser Focus World, 2005. **41**(7): p. 109–114.
38. Hasmemi, S. and W.J.M. Douglas, *Moisture nonuniformity in drying paper: measurement and relation ot process parameters.* Drying Technology, 2003. **21**: p. 329–347.
39. Boulay, R., *et al*., *Paper Sheet Moisture Measurements in the Far Infrared.* International Journal of Infrared and Millimeter Waves, 1984. **5**(9): p. 1221–1234.
40. Banerjel, D., *et al*., *Measurement of paper moisture content using terahertz imaging.* International Paperworld IPW, 2009(12): p. 14021.
41. Hattori, T., H. Kumon, and H. Tamazumi, *Terahertz spectroscopic characterization of paper* in *IRMMW-THz 2010 - 35th International Conference on Infrared, Millimeter, and Terahertz Waves*. 2010. p. Article number 5612460
42. Mousavi, P., *et al*., *Simultaneous composition and thickness measurement of paper using teraherrtz time-domain spectroscopy.* Applied Optics, 2009. **48**(33): p. 6541–6546.
43. Koch, M., *et al*., *THz-imaging: a new method for density mapping of wood.* Wood Science and Technology, 1998. **32**: p. 421–427.
44. Fujii, Y., *et al*., *Nondestructive detection of termites using a millimeter-wave imaging technique.* Forest Products J., 2007. **57**(10): p. 75–79.
45. Fujii, Y., *et al*., *Feasibility of millimeter wave imaging as tool for nondestructive inspection of wood and wooden structures*, in *IRMMW-THz 2010 - 35th International Conference on Infrared, Millimeter, and Terahertz Waves*. 2010. p. Article number 5612351.
46. Oyama, Y., *et al*., *Sub-terahertz imaging of defects in building blocks.* NDT and E International, 2009. **42** (1): p. 28–33.
47. Pereira, H., *Cork: Biology, Production and Uses*. 2007, New York: Elsevier.
48. Rosa, M.E. and M.A. Fortes, Wood and Fiber Science, 1993. **25**: p. 339–348.
49. Gonzalez-Adrados, J.R., *et al*., J. Int. Sci. Vigne Vin, 2008. **42**: p. 161–166.
50. Balakrishnan, J., B.M. Fischer, and D. Abbott, *Sensing the hygroscopicity of polymer and copolymer materials using terahertz time-domain spectroscopy.* Applied Optics, 2009. **48**(12): p. 2262–2266.
51. Hejase, J.A., P.R. Paladhi, and P. Chahal, *Terahertz Packaging: Study of Substrates for Novel Component Designs*, in *2010 Electronics Components and Technology Conference*. 2010. p. Article number 5490763 Pages 744–751.
52. Pasupuleti, R., *et al*., *Modelling of moisture diffusion in multilayer woven fabric composites.* Computational Materials Science, 2011. **50**: p. 1675–1680.

53. Wietzke, S., *et al*., *Terahertz Spectroscopy A Powerful Tool for the Characterization of Plastic Materials*, in *2010 International Conference on Solid Dielectrics*. 2010: Potsdam, Germany. p. 1–4.
54. Hadjiloucas, S., L.S. Kratzas, and W.J. Bowen, *Measurement of leaf water content using terahertz radiation.* IEEE Trans. Microwave Theory Tech. , 1999. **47**: p. 142–149.
55. Zhang, H., K. Mitobe, and N.Yoshimura. *Terahertz imaging for water content measurement*. in *Proceedings of 2008 International Symposium on Electrical Insulating Materials*. 2008. Yokkaichi, Mie, Japan.
56. Ogawa, Y., *et al*., *Nondestructive and Real-time Meaurement of Moisture in Plant.* IEEJ Trans. EIS, 2004. **124**(9): p. 1672–1677.
57. Hadjiloucas, S., R.K.H. Galvao, and J.W. Bowen, *Analysis of spectroscopic measurements of leaf water content at terahertz frequencies using linear transforms.* J. Opt. Soc. Am. A, 2002. **19**(12): p. 2495–2509.
58. Hadjiloucas, S., *et al*., *Propagation of errors from a null balance terahertz reflectometer to a sample's relative water content.* Journal of Physics: Conference Series, 2009. **178**: p. 012012.
59. Ung, B.S.-Y., *et al*., *Towards Quality Control of Food Using Terahertz.* Proceedings of SPIE, 2008. **6799**: p. 67991E.
60. Labuza, T.P. and C.R. Hyman, *Moisture migration and control in multi-domain foods.* Trends in Food Science & Technology, 1998. **9**: p. 47–55.
61. Parasoglou, P., *et al*. *Quantitative moisture content detection in food wafers*. in *34th International Conference on Infrared, Millimeter, and Terahertz Waves, IRMMW-THz 2009*. 2009.
62. Parasoglou, P., *et al*., *Quantitative Water Content Measurements in Food Wafers Using Terahertz Radiation.* Terahertz Science and Technology, 2010. **3**(4): p. 1–11.
63. Li, B., *et al*., *Preliminary study on quality evaluation of pecans with terahertz time-domain spectroscopy.* Proc. SPIE, 2010. **7854**: p. 78543 V.
64. Chua, H.S., *et al*., *Terahertz time-domain spectroscopy of crushed wheat grain*, in *IEEE MTT-S International Microwave Symposium Digest*. 2005. p. art. no. 1517162, pp. 2103–2106.
65. Ogawa, Y., *et al*., *Feasibility on the quality evaluation of agricultural products with terahertz electromagnetic wave*, in *2006 ASABE Annual International Meeting*. 2006: Portland, Oregon. p. Paper Number: 063050.
66. Federici, J.F., *et al*., *Application of terahertz Gouy phase shift from curved surfaces for estimation of crop yield.* Applied Optics, 2009. **48**(7): p. 1382–1388.
67. Howell, G.S., C. Schutte, and J. Treloar, *Crop Estimation and Sampliing to Achieve Optimal Fruit Maturity and Quality under Michigan Conditions*, in *Final Report to Michigan Grape and Wine Industry Council, Research and Education Advisory Committee*. 2006.
68. Siegman, S.E., *Lasers*. 1986: University Science Books.
69. Ruffin, A.B., *et al*., *Direct Obwervation of the Gouy Phase SHift with Single-Cycle Terahertz Pulses.* Phys. Rev. Lett., 1999. **83**: p. 3410–3413.
70. Takeshi Yasui, T.Y., Ken-ichi Sawanaka, and Tsutomu Araki, *Terahertz paintmeter for noncontact monitoring of thickness and drying progress in paint film.* Applied Optics, 2005. **44**(32): p. 6849–6856.
71. Yasuda, T., *et al*., *Real-time two-dimensional terahertz tomography of moving objects.* Optics Communications, 2006. **267**: p. 128–136.
72. Fukunaga, K., *et al*., *Terahertz imaging systems: a non-invasive technique for the analysis of paintings.* Proc. of SPIE, 2009. **7391**: p. 93910D.
73. Jackson, J.B., *et al*., *Terahertz pulse imaging for tree-ring analysis: a preliminary study for dendrochronology applications.* Meas. Sci. Technol., 2009. **20**: p. 075502.
74. Maruyama, I., N. Kishi, and K. Kawase, *Measurement of water content in hardened cement paste using Terahertz radiation*. Journal of Structural and Construction Engineering (Transactions of AIJ), 2010. **75** (652): p. 1073–1079.